IUCrJ
ISSN 2052-2525
CHEMISTRY | CRYSTENG

Hierarchical dielectric orders in layered ferroelectrics Bi_2SiO_5

Younghun Kim,[a,b] Jungeun Kim,[b,c] Akihiko Fujiwara,[c] Hiroki Taniguchi,[d] Sungwng Kim,[e] Hiroshi Tanaka,[f] Kunihisa Sugimoto,[b,c] Kenichi Kato,[b] Mitsuru Itoh,[g] Hideo Hosono[g,h] and Masaki Takata[a,b,c]*

[a]Department of Advanced Materials Science, The University of Tokyo, Kashiwa, Chiba 277-8561, Japan, [b]RIKEN SPring-8 Center, Kouto, Sayo-cho, Hyogo 679-5148, Japan, [c]Japan Synchrotron Radiation Research Institute, Kouto, Sayo-cho, Hyogo 679-5148, Japan, [d]Department of Physics, Nagoya University, Furo-cho, Nagoya 464-8602, Japan, [e]Department of Energy Science, Sungkyunkwan University, Jangan-Gu, Suwon 440-746, South Korea, [f]Department of Materials Science, Shimane University, 1060 Nishi-kawatsu-cho, Matsue, Shimane 690-8504, Japan, [g]Materials and Structures Laboratory, Tokyo Institute of Technology, Yokohama 226-8503, Japan, and [h]Frontier Research Center, Tokyo Institute of Technology, Yokohama 226-8503, Japan. *Correspondence e-mail: takatama@spring8.or.jp

Received 3 December 2013
Accepted 10 April 2014

Edited by I. Robinson UCL, UK

Keywords: electron charge density; electrostatic potential; visualization of local polarization; hierarchical dielectric ordering

Supporting information: this article has supporting information at www.iucrj.org

Electric dipole engineering is now an emerging technology for high electron-mobility transistors, ferroelectric random access memory and multiferroic devices *etc.* Although various studies to provide insight into dipole moment behaviour, such as phase transition, order and disorder states, have been reported, macroscopic spontaneous polarization has been mainly discussed so far. Here, visualization of the electric dipole arrangement in layered ferroelectrics Bi_2SiO_5 by means of combined analysis of maximum entropy charge density and electrostatic potential distribution analysis based on synchrotron radiation X-ray powder diffraction data is reported. It was found that the hierarchical dipole orders, the weak-ferroelectric and ferroelectric configurations, were observed in the Bi_2O_2 and the SiO_3 layers, respectively, and the ferrielectric configuration was realised by the interlayer interaction. This discovery provides a new method to visualize the local polarization in ferroelectric materials.

1. Introduction

Designing and controlling the intense local electric field and/or polarization in solids is vital for emerging electronics, such as high-performance field-effect transistors, ferroelectric random access memory and multiferroic devices in the nanoscale (de Araujo *et al.*, 1995; Auciello *et al.*, 1998; Haertling, 1999; Scott, 2000; Dawber *et al.*, 2005; Schilling *et al.*, 2007; Chung *et al.*, 2011; Yamada *et al.*, 2012; Keeney *et al.*, 2012*a*,*b*, 2013; Maity *et al.*, 2012; Zhang *et al.*, 2012). Dielectric properties have been mainly discussed in terms of macroscopic properties based on measurements of dielectric permittivity (ε) and electric polarization (P) under electric fields (E) for bulk samples so far. Recently, electrostatic potential (EP) analysis based on electron charge density (ECD) using the maximum entropy method (MEM) has been developed for the characterization of specific features originating from the electrostatic field/force on the microscopic scale (Sakata & Sato, 1990; Takata & Sakata, 1996; Takata, 2008; Tanaka *et al.*, 2006; Kim *et al.*, 2011). Using ECD/EP analysis, we succeeded in visualizing the relationship between internal electric fields and physical properties, such as thermal conductivity affected by rattling (Fujiwara *et al.*, 2012) and superconductivity related to the bi-polaron (Kim *et al.*, 2014).

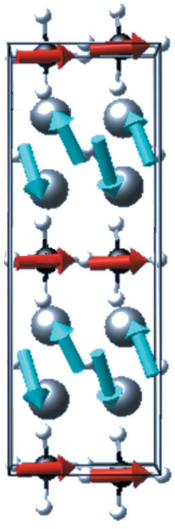

Bi_2SiO_5 (BSO) has attracted much attention as an alternative to the traditional lead-based ferroelectric materials with a phase-transition temperature (T_c) of 673 K. BSO has an Aurivillius-like structure consisting of the $[Bi_2O_2]^{2+}$ layer and $[SiO_3]^{2-}$ layer (Fig. 1*a*) (Pirovano *et al.*, 2001; Georges *et al.*, 2006; Taniguchi *et al.*, 2013). A relatively large spontaneous polarization (P_c) of 14.5 μC cm^{-2} along the SiO_3 chain (*c*-axis) was predicted by first-principles calculations, while those along the *a*- and *b*-axes, P_a and P_b, are estimated to be small, 0.1 μC cm^{-2} and 0 μC cm^{-2}, respectively (Taniguchi *et al.*, 2013). From experimental *P versus E* measurements (Taniguchi *et al.*, 2013), only the P_a value of 0.8 μC cm^{-2} was detected, because the BSO crystals have a thin-plate shape, and the electrode for the *P versus E* measurements can only be formed on a large area of the *b*–*c* plane of the crystals. In addition, the polarization of BSO is suggested to originate from the SiO_3 layer and not from the Bi_2O_2 layer by the first-principles calculations (Taniguchi *et al.*, 2013). Clarification of the origin and mechanism of the ferroelectricity in BSO is therefore crucial for further development of lead-free ferroelectric materials.

Here, we report the visualization of the electric dipole arrangement in layered ferroelectrics Bi_2SiO_5 by means of combined analysis of the ECD using MEM and EP distribution analysis based on high-precision synchrotron radiation X-ray powder diffraction data.

2. Experimental

Synchrotron radiation X-ray powder diffraction measurements of BSO were performed at BL02B2 beamline at SPring-8 with a large Debye–Scherrer camera to obtain high counting statics for accurate structure analysis (Nishibori *et al.*, 2001; Takata *et al.*, 2002). The BSO sample was sufficiently ground for a homogeneous distribution of intensity and sealed in a glass capillary with a diameter of 0.1 mm. The diffraction pattern was measured at 300 K and 773 K with a N_2 gas flowing temperature control system. The measurement wavelength was 0.35206 (1) Å to reduce absorption effects caused by the heavy atom (Bi) in the sample. The diffraction data were collected for 45 min on an image plate installed in the large Debye–Scherrer camera.

Determination of the precise structure was carried out by Rietveld refinement. Details of the process and the results are described in the supporting information. The total number of observed structure factors was 3921 and 2930 at 300 K and 773 K, respectively. The ECD was calculated by MEM using the *ENIGMA* program (Sakata *et al.*, 1990; Tanaka *et al.*, 2002). The electrostatic potential was calculated with a method developed by Tanaka *et al.* using the MEM electron charge density (Tanaka *et al.*, 2006). The electrostatic potential $[U(r)]$ is composed of the nucleus charge $[U_{nuc}(r)]$ and the electron charge $[U_{ele}(r)]$ components. In this study, ECD and EP were visualized using the *OpenDx* program provided by IBM Visualization Data Explorer. The procedure for the polarization calculations is described in the supporting information.

3. Results

The ECD/EP analysis is one of the best ways to understand the microscopic behaviour of polarizations in BSO. The ECD distributions directly obtained from integrated intensities of the X-ray diffraction pattern by MEM analysis reveal the deformation of both the BiO_4 square pyramids in the Bi_2O_2 layer and the SiO_3 tetrahedra in the SiO_3 layer [Figs. 1(*b*)–1(*e*)]. In the ferroelectric phase (300 K), the Bi atoms form a stronger covalent bond with one of the four equivalent first-

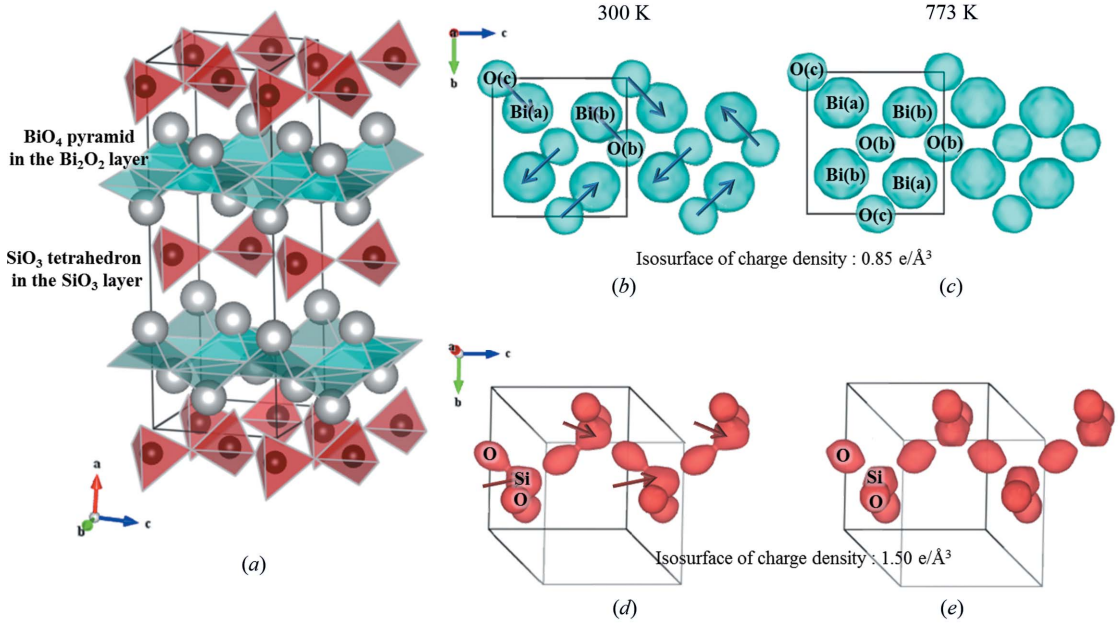

Figure 1
Schematic drawing of the crystal structure (*a*) and ECD using MEM distribution of the Bi_2O_2 (*b*, *c*) and the SiO_3 layer (*d*, *e*) in the ferroelectric (300 K) and paraelectric (773 K) phases. The isosurface of ECD is 0.85 e Å^{-3} and 1.50 e Å^{-3} for the Bi_2O_2 and the SiO_3 layer, respectively.

neighbour O atoms in the paraelectric phase (773 K) (see Fig. S4 and Table S4 of the supporting information). The Bi(*b*)–O(*b*) and Bi(*a*)–O(*c*) pairs form electric dipole moments, and the two neighbouring electric dipoles form an almost antiparallel configuration in the Bi_2O_2 layer (Fig. 1*b*). On the other hand, the Si atoms in the ferroelectric phase form a stronger covalent bond (Fig. 1*d*) with three of the four equivalent first-neighbour O atoms in the paraelectric phase (Fig. 1*e*), showing that the SiO_3 cluster has an electric dipole moment. The electric dipoles of SiO_3 align in the ferroelectric configuration. From the ECD analysis using MEM, the results visualized the antiferroelectric order in the Bi_2O_2 layer and the ferroelectric order in the SiO_3 layer in the ferroelectric phase, as shown in Figs. 2(*a*) and 2(*b*). This is the reason why the large dipole moment of BSO originates from the SiO_3 layer instead of the Bi_2O_2 layer.

Electric dipole moments in the crystal can be calculated from the electron charge using MEM and the nuclear charge using Ewald's method. It is, however, well known that the value of the polarization calculated from the charge distribution strongly depends on the method of selection of the crystallographic unit cell: the determination of the boundary of the crystallographic unit cell is critical for the calculation (Resta & Vanderbilt, 2007; Spaldin, 2012). This issue can be resolved by the Berry-phase theory (King-Smith & Vanderbilt, 1993; Resta, 1994; Neaton *et al.*, 2005). In the current case, we introduce the concept of fragments for extracting experimentally individual dipole units originating from BiO and SiO_3 clusters. The boundary of fragments can be determined by the local minimum value of EP around the fragments (ECD/EP method) so that each fragment satisfies charge neutrality. An extracted fragment unit of SiO_3 is shown in Fig. 3 as an example. The partial electric polarization in the fragments can be estimated by (Spaldin, 2012; Gohda *et al.*, 2000)

$$\mathbf{P} = \frac{e}{V}\Big\{\sum_i A_i\big[(X_i - x_o)\hat{x} + (Y_i - y_o)\hat{y} + (Z_i - z_o)\hat{z}\big] - \Big[\int (x_i - x_o)\rho_i(x_i)\,\mathrm{d}x_i\,\hat{x} + \int (y_i - y_o)\rho_i(y_i)\,\mathrm{d}y_i\,\hat{y} + \int (z_i - z_o)\rho_i(z_i)\,\mathrm{d}z_i\,\hat{z}\Big]\Big\}, \quad (1)$$

where V is the volume of the unit cell; e is the elementary charge (1.602×10^{-19} C); A_i is atomic number; (X_i, Y_i, Z_i) is the position of ith atom; (x_o, y_o, z_o) is the position of the center of mass in the fragment unit; $\rho_i(x_i, y_i, z_i)$ is the electron density located at the ith pixel; (x_i, y_i, z_i) is the position of ith pixel for electron charge contribution; $(\hat{x}, \hat{y}, \hat{z})$ is the unit vector. Integration is carried out over the fragment unit; the value of the electron density is assigned to pixels in a unit cell divided into $256 \times 128 \times 128$ pixels. The total and projected values of polarization are summarized in Table 1.

The SiO_3 layer shows a large polarization along the *c*-axis originating from a large dipole moment of the SiO_3 fragment [27.3 (1) μC cm^{-2}]. The projected values of the polarization along the *a*- and *c*-axis, P_a and P_c, in the SiO_3 layer are 1.4 (1) μC cm^{-2} and 27.3 (1) μC cm^{-2}, respectively. It should be noted that P_b is zero due to the inversion symmetry operation along the *b*-axis. On the other hand, the Bi_2O_2 layer has a small but distinct polarization value in spite of the antiferroelectric order: the projections of the polarization in the Bi_2O_2 layers were −1.8 (1) μC cm^{-2} for P_a and −3.8 (1) μC cm^{-2} for P_c. This originates from the asymmetric distortion of the Bi_2O_2 pyramids, meaning that the Bi–O dipoles with antiparallel configuration do not fully cancel out the polarization in the layer: this is regarded as the weak-ferroelectric configuration, as shown in Fig. 2(*c*). Since the residual polarization in the Bi_2O_2 layer aligns in the antiparallel direction to the polarization in the SiO_3 layer, the distortion in the Bi_2O_2 layer is suggested to be induced by the large polarization of the SiO_3 layer for reducing the electrostatic energy in the crystal. The individual dipole moment [26.8 (3) μC cm^{-2} and 27.0 (4) μC cm^{-2}] of Bi–O is comparably large with that of the SiO_3 fragment [27.3 (1) μC cm^{-2}], although the net value is as small as 4.2 (1) μC cm^{-2} owing to the antiparallel configuration of the Bi–O dipoles.

The total P_a and P_c of BSO were estimated to be 0.3 (2) μC cm^{-2} and

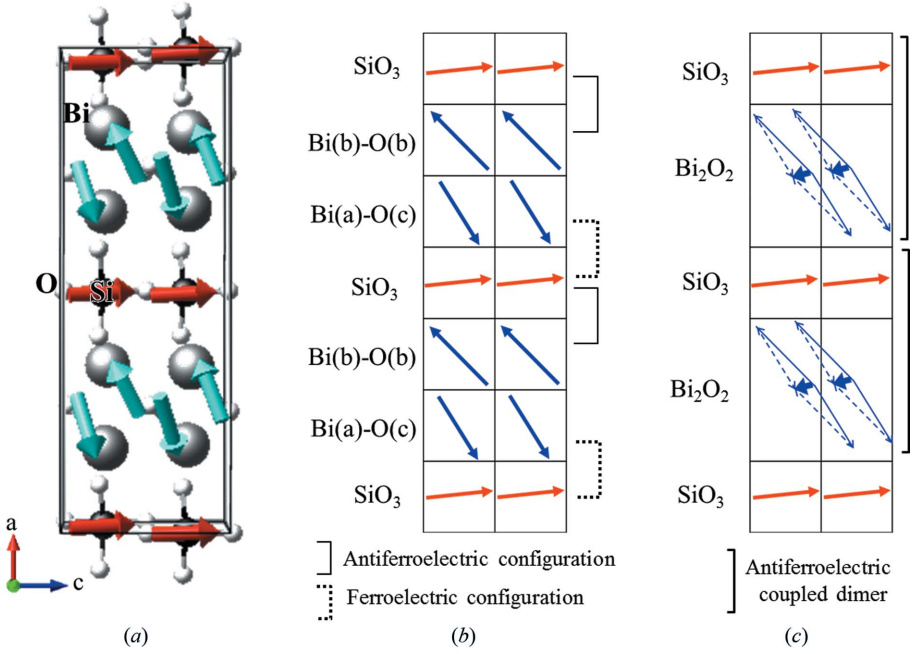

Figure 2
Schematic of the electric dipole configuration of Bi_2SiO_5 based on the polarization obtained by the ECD/EP method. (*a*) Three-dimensional electric dipole configuration with atom positions. (*b*) Schematics of dipole ordering for SiO_3, Bi(*b*)–O(*b*) and Bi(*a*)–O(*c*). (*c*) Schematic dipole ordering showing a weak-ferroelectric configuration of the Bi_2O_2 layer. The residual dipole in the Bi_2O_2 layer is aligned antiparallel to the large dipole in the SiO_3 layer showing the ferrielectric configuration.

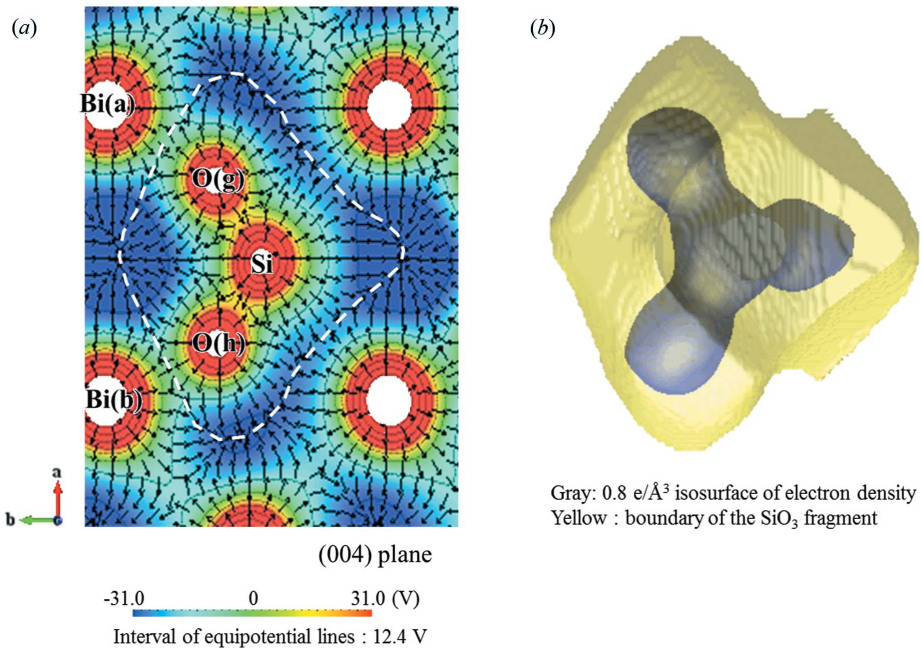

Figure 3
Extracted SiO_3 fragment. (*a*) Two-dimensional EP map on the (004) plane with electric fields. The boundary defining the dipole unit can be determined by the local minimum value of the EP around the fragments (white dashed line). (*b*) Extracted three-dimensional perspective of the SiO_3 fragment area (yellow) with the shape of the SiO_3 molecule with an isosurface of 0.8 e Å^3 (grey).

23.5 (1) μC cm^{-2}, respectively. P_b was zero because of the symmetry operation of the crystal structure. The value of P_a is roughly consistent with that predicted by theoretical calculation (0.1 μC cm^{-2}) and that determined by *P versus E* measurements (0.8 μC cm^{-2}) (Taniguchi *et al.*, 2013). In addition, the large P_c value predicted by theoretical calculation [14.5 μC cm^{-2}] was experimentally determined by a microscopic approach using ECD/EP analysis [23.5 (1) μC cm^{-2}]. The result shows that the ECD/EP analysis using precise X-ray diffraction data can derive the local electric dipole moment in the crystal as well as in the polarization values from small amounts (less than 0.1 mg) of powder samples, and values are consistent with those predicted by the complete picture based on the Berry-phase theory. It should be noted that the values of polarization based on the point charge model, where the electron charge of atoms was assigned to each atomic position obtained by Rietveld analysis, largely deviated from any other results of theoretical prediction, *P versus E* measurements and the ECD/EP analysis; this result shows that the use of the ECD distribution is essential for estimation of accurate values of polarization. The method of ECD/EP analysis is, therefore, useful for characterization and design of newly synthesized dielectric materials, and thus for the development of emerging dielectric materials.

The hierarchical dipole ordering with structural distortion can be understood in terms of electrostatic energy. Firstly, the antiferroelectric configuration with the residual dipole moments (weak ferroelectricity) and the ferroelectric configuration are realised in the Bi_2O_2 and the SiO_3 layer, respectively. Next, the antiparallel arrangement between the net small dipoles in the Bi_2O_2 layer and the large dipoles in the SiO_3 layers reduces the interlayer electrostatic interaction; this configuration is regarded as an interlayer ferrielectric ordering. In addition, the neighbouring Bi_2O_2 and SiO_3 layers form a pair, namely, the dimerization of the layers (Figs. 2*c* and S3*a*). In this distortion the dipoles in the neighbouring layer being aligned in the antiparallel configuration become close to reduce the electrostatic energy. In actual fact, the cohesive energy of the low-temperature 'ferroelectric' phase is lower than that of the high-temperature paraelectric phase by 23.1 meV in Bi_2SiO_5 (Taniguchi *et al.*, 2013), showing an energetic advantage of the 'ferroelectric' phase with hierarchical dipole ordering.

The ECD/EP analysis can visualize the properties of covalency and polarization in the crystal using a tiny amount of powder sample. In addition, the method demonstrates its ability to visualize local polarization which cannot be detected by the macroscopic measurements in principle. In the case of BSO, for instance, a large dipole moment should be induced at the SiO_3 layer, and large polarization is stabilized by the antiparallel configuration with the Bi_2O_2 layer.

Table 1
Total and projected polarization estimated by the ECD/EP method, point charge model (PC model), *P versus E* measurement and first-principles calculation.

P versus E measurements and the first-principles calculation are reported by Taniguchi *et al.* (2013). All values are shown in units of μC cm^{-2}.

		Total polarization	Projected polarization		
		$\|P\|$	P_a	P_b	P_c
ECD/EP method	Bi_2O_2 layer	4.2 (1)	−1.8 (1)	0	−3.8 (1)
	Bi(*b*)–O(*b*) sublayer (upper square-pyramid component)	26.8 (3)	24.0 (3)	0	−11.9 (1)
	Bi(*a*)–O(*c*) sublayer (lower square-pyramid component)	27.0 (4)	−25.8 (4)	0	8.0 (1)
	SiO_3 layer	27.3 (1)	1.4 (1)	0	27.3 (1)
	Bi_2SiO_5	23.5 (1)	0.3 (2)	0	23.5 (1)
PC model	Bi_2SiO_5	9.4	4.9	0	8.1
P versus E measurement	Bi_2SiO_5	–	0.8	–	–
First-principles calculation	Bi_2SiO_5	14.5	0.1	0	14.5

4. Summary

In summary, we have discovered a new approach to the visualization of the local electric dipole moments and their orders in a crystal by means of the combined analysis of ECD using MEM and EP distribution analysis based on synchrotron radiation X-ray powder diffraction data. Application of this method revealed hierarchical dipole ordering in Bi_2SiO_5: the weak ferroelectricity in the Bi_2O_2 layer, the ferroelectric order in the SiO_3 layer, and the ferrielectric order between the Bi_2O_2 and SiO_3 layers. The results suggest that ECD/EP analysis is a useful method to visualize the local polarization based on X-ray powder diffraction experiment.

Acknowledgements

The X-ray diffraction data were measured at BL02B2 (proposal Nos. 2010B2034 and 2011B2089) of SPring-8. This work was supported in part by RIKEN International Program Associate (IPA), a Grant-in-Aid for Molecular System Research in RIKEN, MEXT Element Strategy Initiative to Form Core Research Centers, and the Ministry of Education, Culture, Sports, Science and Technology of Japan through a Giant-in-Aid for Young Scientists (B, No. 24760543).

References

Araujo, C. A. P. de, Cuchiaro, J. D., McMillan, L. D., Scott, M. C. & Scott, J. F. (1995). *Nature (London)*, **374**, 627–629.
Auciello, O., Scott, J. F. & Ramesh, R. (1998). *Phys. Today*, **51**, 22–27.
Chung, Y., Verploegen, E., Vailionis, A., Sun, Y., Nishi, Y., Murmann, B. & Bao, Z. (2011). *Nano Lett.* **11**, 1161–1165.
Dawber, M., Rabe, K. M. & Scott, J. F. (2005). *Rev. Mod. Phys.* **77**, 1083–1130.
Fujiwara, A., Sugimoto, K., Shih, C. H., Tanaka, H., Tang, J., Tanabe, Y., Xu, J., Heguri, S., Tanigaki, K. & Takata, M. (2012). *Phys. Rev. B*, **84**, 144305.
Georges, S., Goutenoire, F. & Lacorre, P. (2006). *J. Solid State Chem.* **179**, 4020–4028.
Gohda, T., Ichikawa, M., Gustafsson, T. & Olovsson, I. (2000). *Acta Cryst.* B**56**, 11–16.
Haertling, G. H. (1999). *J. Am. Ceram. Soc.* **82**, 797–818.
Keeney, L., Groh, C., Kulkarni, S., Roy, S., Pemble, M. E. & Whatmore, R. W. (2012*a*). *J. Appl. Phys.* **112**, 024101.
Keeney, L., Kulkarni, S., Deepak, N., Schmidt, M., Petkov, N., Zhang, P. F., Cavill, S., Roy, S., Pemble, M. E. & Whatmore, R. W. (2012*b*). *J. Appl. Phys.* **112**, 052010.
Keeney, L., Maity, T., Schmidt, M., Amann, A., Deepak, N., Petkov, N., Roy, S., Pemble, M. E. & Whatmore, R. W. (2013). *J. Am. Ceram. Soc.* **96**, 2339–2357.
Kim, J., Fujiwara, A., Sawada, T., Kim, Y., Sugimoto, K., Kato, K., Tanaka, H., Ishikado, H., Shamoto, S. & Takata, M. (2014). *IUCrJ*, **1**, 155–159.
Kim, J., Kato, K., Takata, M., Shibata, T. & Moritomo, Y. (2009). *Phys. Rev. B*, **79**, 132105.
Kim, J., Tanaka, H., Kato, K., Takata, M. & Moritomo, Y. (2011). *Appl. Phys. Express*, **4**, 025801.
King-Smith, R. D. & Vanderbilt, D. (1993). *Phys. Rev. B*, **47**, 1651–1654.
Maity, T., Li, S., Keeney, L. & Roy, S. (2012). *Phys. Rev. B*, **86**, 024438.
Neaton, J. B., Ederer, C., Waghmare, U. V., Spaldin, N. A. & Rabe, K. M. (2005). *Phys. Rev. B*, **71**, 014113.
Nishibori, E., Takata, M., Kato, K., Sakata, M., Kubota, Y., Aoyagi, S., Kuroiwa, Y., Yamakata, M. & Ikeda, N. (2001). *Nucl. Instrum. Methods Phys. Res. A*, **467–468**, 1045–1048.
Pirovano, C., Islam, M. S., Vannier, R. N., Nowogrocki, G. & Mairesse, G. (2001). *Solid State Ion.* **140**, 115–123.
Resta, R. (1994). *Rev. Mod. Phys.* **66**, 899–915.
Resta, R. & Vanderbilt, D. (2007). *Top. Appl. Phys.* **105**, 31–68.
Sakata, M., Mori, R., Kumazawza, S., Takata, M. & Toraya, H. (1990). *J. Appl. Cryst.* **23**, 526–534.
Sakata, M. & Sato, M. (1990). *Acta Cryst.* A**46**, 263–270.
Schilling, A., Bowman, R. M., Catalan, G., Scott, J. F. & Gregg, J. M. (2007). *Nano Lett.* **7**, 3787–3791.
Scott, J. F. (2000). *Ferroelectric Memories.* Heidelberg: Springer.
Spaldin, N. A. (2012). *J. Solid State Chem.* **195**, 2–10.
Takata, M. (2008). *Acta Cryst.* A**64**, 232–245.
Takata, M., Nishibori, E., Kato, K., Kubota, Y., Kuroiwa, Y. & Sakata, M. (2002). *Adv. X-ray Anal.* **45**, 377.
Takata, M. & Sakata, M. (1996). *Acta Cryst.* A**52**, 287–290.
Tanaka, H., Kuroiwa, Y. & Takata, M. (2006). *Phys. Rev. B*, **74**, 172105.
Tanaka, H., Takata, M., Nishibori, E., Kato, K., Iishi, T. & Sakata, M. (2002). *J. Appl. Cryst.* **35**, 282–286.
Taniguchi, H., Kuwabara, A., Kim, J., Kim, Y., Moriwake, H., Kim, S., Hoshiyama, T., Koyama, T., Mori, S., Takata, M., Hosono, H., Inaguma, Y. & Itoh, M. (2013). *Angew. Chem. Int. Ed.* **52**, 8088–8092.
Toby, B. H. (2006). *Powder Diffr.* **21**, 67–70.
Yamada, H., Yoshimura, T. & Fujimura, N. (2012). *Jpn. J. Appl. Phys.* **51**, 11PB01.
Zhang, P. F., Deepak, N., Keeney, L., Pemble, M. E. & Whatmore, R. W. (2012). *Appl. Phys. Lett.* **101**, 112903.